Research Article

In-situ synthesis of mixed phase electrospun TiO_2 nanofibers: a novel visible light photocatalyst

Jyoti Prakash Dhal[1,2] · Shraban Kumar Sahoo[2] · Sandip Padhiari[2] · Tapan Dash[3] · Garudadhwaj Hota[2]

© Springer Nature Switzerland AG 2019

Abstract

TiO_2 nanofibers were synthesized by electrospinning method using mixed titanum isopropoxide and polyvinylpyrrolidone precursors in ethanol followed by calcination at high temperature. The obtained TiO_2 e-spun nanofibers were characterized by FESEM, TEM, XRD, XPS and BET surface area analytical techniques. XRD result shows that the nanofibers contain both anatase and rutile mixed phases. FESEM and TEM study indicates the development of precise fine tiny nanoparticles with diameter in the range of 10–20 nm, which are oriented along one dimensional direction to form the fibrous structure with diameter in the range of 300–500 nm. The mixed phase TiO_2 nanofibers were used as photocatalysts for degradation of Rhodamine-B and Methyl orange under solar light irradiation and also under visible light irradiation. More than 99% degradation was achieved within 90 min of irradiation time for both the dyes. Furthermore, it is observed that the TiO_2 photocatalyst is efficiently degrading (98%) the tetracycline hydrochloride solution within 70 min of contact time. The excellent visible light photocatalytic activity may be attributed to the combine factors of hetero-conjunction at anatase–rutile interface and immediate charge transfer due to 1D structure, which inhibit the electron–hole recombination.

Graphical abstract Rutile-Anatase dual phase TiO2 nanofibers exhibit excellent visible light photocatalytic activity due to the combine factors of hetero-conjunction at anatase-rutile interface and immediate charge transfer due to 1D structure, which inhibits the electron-hole recombination.

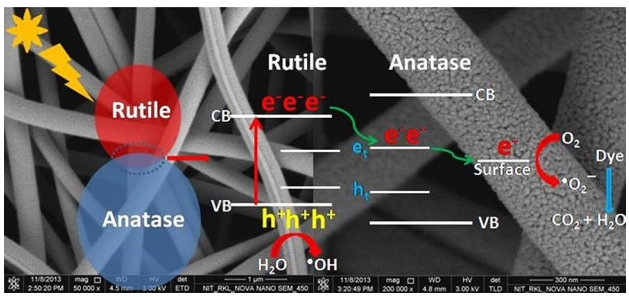

Keywords Electrospinning · Anatase · Rutile · Nanofibers · Photocatalysts

Electronic supplementary material The online version of this article (https://doi.org/10.1007/s42452-019-0261-6) contains supplementary material, which is available to authorized users.

✉ Jyoti Prakash Dhal, jyoti84.chem@gmail.com; ✉ Garudadhwaj Hota, garud31@yahoo.com; garud@nitrkl.ac.in | [1]Department of Chemistry, College of Engineering and Technology, B.P.U.T, Bhubaneswar, Odisha 751003, India. [2]Department of Chemistry, National Institute of Technology, Rourkela, Odisha 769008, India. [3]Department of Physics, Centurion University of Technology and Management (CUTM), Bhubaneswar, Odisha 752050, India.

SN Applied Sciences (2019) 1:243 | https://doi.org/10.1007/s42452-019-0261-6

Received: 5 January 2019 / Accepted: 14 February 2019 / Published online: 19 February 2019

1 Introduction

The textile industries utilize about 10,000 dyes and pigments. Wastewaters from printing and dyeing units of the industries are highly hazardous to aquatic living and human beings because they cause serious damage to the surrounding environment [1–3]. Thus, it is very essential to remove it from water. Many technologies have been proposed for the treatment of dyeing effluents, including biological, adsorption, membrane and chemical oxidation. However, these technologies still have some problems such as secondary pollution or insufficient treatment. Removal of toxic dyes by photocatalysis with semiconductors is widely investigated as a useful technique not only for the efficient degradation of contaminants in waste water, but also for utilization of abundant solar energy without the need for additional chemical regents [4, 5].

Among the photoactive semiconductors, nanostructured TiO_2 has received a great attentation as a photocatalyst due to its suitable band structure, high chemical and thermal stability, non-environmental effect and low cost [6–8]. However, there are several limitations like low absorbance in visible reason, high recombination rate of photo generated electron–hole pairs which restricts its practical application as an efficient photocatalyst [9]. Therefore, there is a need for the development of visible light responsive photocatalyst. Recently many efforts have been taken to improve the visible light active photocatalytic properties of TiO_2 such as by doping with metals [10–14] and nonmetals [15–18], deposition of noble metals [19–21], surface fluorination [22] and controlling crystal facets [23], by creating heterojunction by coupling with other semiconductor materials having suitable band gap [24–28]. Design of nano structures having different morphologies like nanoflower [29], nanofibers [30], nanorod [31], coupling with carbanious materials like grapheme [32], carbon nanotube [33], and development of porous nanostructures [19] have also been proposed to increase visible light absorbance and to reduce the electron–hole pair recombination rate of TiO_2.

Apart from this, development of 1D TiO_2 nanomaterials has received great attention throughout the field. It is because 1D TiO_2 nanostructures cannot only improve light absorption but also can reduce electron–hole pair recombination rate. The reasons behind the extraordinary properties of 1D nanostructure over nanoparticles are: faster electron diffusion than in nanoparticles; presence of additional energetic barrier to recombination due to the formation of a space-charge region; 1D nanofibers ensure the rapid collection of carriers generated by the reducing surface [34–36].

It is well known that TiO_2 exists in three structural forms namely anatase (3.2 eV), rutile (3.0 eV) and brookite (3.4 eV) [37]. Among these forms inspite of larger band gap anatase exhibits better photocatalytic activity than rutile because anatase has unique ability to separate photo generated electron hole pairs more than rutile. It has been reported that creating a heterojunction with anatase and rutile phase exhibits higher photo catalytic activity than individual pure anatase and rutile structures. Unlike the normal heterojunction, due to proper alignment of energy levels and similarity of crystal lattice, formation of heterojunction between two TiO_2 based materials can prevent formation of charge transfer barrier at the heterojunction interface [38]. Thus developing 1D TiO_2 nanomaterials in which there exist a heterojunction between anatase and rutile can generate highly efficient visible light responsive photocatalyst.

Electrospinning is an effective, straightforward, and convenient method to synthesize continuous semiconductor metal oxide nanofiber photocatalysts with high photocatalytic activity and favorable recycling characteristics due to their one dimensional (1D) nanostructural property [39, 40]. Metal oxide nanofibers are usually prepared by electrospinning a precursor metal salt solution with the help of a proper polymer, followed by calcination to decompose the polymer completely and turn metal salt into metal oxide [41].

In this work, we have reported an efficient method for the fabrication of TiO_2 nanofibers by calcination of electrospun PVP/$Ti(OiPr)_4$ composite nanofibers at 500 °C for 2 h. The photocatalytic ability of prepared TiO_2 nanofibers was investigated by degradation of organic dyes, Rhodamine-B and Methyl orange under solar light irradiation and the photo-degradation process was detected using a simple UV–Vis spectroscopy method.

2 Experimental techniques

2.1 Materials

Polyvinylpyrrolidone (PVP) (Mw ca. 1,300,000), titanumisopropoxide (TIP), acetic acid, ethanol, Rhodamine-B and Methyl orange dyes were commercially available and used as received.

2.2 Methods

2.2.1 Synthesis of electrospun TiO_2 nanofibers

In a typical synthesis procedure 0.5 g of ethanol, 0.5 g of acetic acid and 0.5 g of Titanumisopropoxide (TIP) were mixed and stirred for 10 min to form Solution-A. 0.24 g of

PVP dissolved in 1.2 g of ethanol to form Solution-B. Then solution A was added to solution B with constant stirring and the stirring was continued for 2 h after stirring to get uniform composite solution. Then the prepared solution was delivered to a stainless needle with inner diameter: 0.5 mm) at a constant flow rate of 1.0 mL/h by a plastic syringe pump. As a high voltage of 13 kV was applied, the precursor solution jet accelerated towards the cathode which was placed 10 cm from the needle tip, leading to the formation of nanofiber arrays onto the aluminum foil substrate accompanied by solvent evaporation to form PVP/TIP nanofiber. The as-spun nanofibers were then calcined at 500 °C in air for 2 h to form ultrafine TiO_2 nanofiber.

2.2.2 Nanofiber characterization

The morphologies of the as-fabricated nanofibers were observed by FESEM (Nova Nano SEM 450) and transmission electron microscopy (TEM; JEM-2100 HRTEM, Make-JEOL, Japan). The crystal structure of the nanofibers was identified by XRD pattern recorded on a Rigaku Ultima-IV X-ray diffractometer with Cu Kα radiation (λ = 1.54156 Å) at a scan rate of 5°/min in the range of 20°–80°. X-ray photoelectron spectroscopy (XPS) was determined using a VG Scientific ESCA LAB Mk-II Spectrometer with Al Kα radiation (1486.6 eV) at a takeoff angle at 45°. The UV–Visible absorbance spectra of the nanofibers were analyzed with Shimadzu spectrometer (model 2450) with $BaSO_4$ coated integration sphere within the range 200–800 nm. Specific surface area and pore size distribution (PSD) of the nanofibers were determined from nitrogen adsorption/desorption isotherms obtained at the temperature of liquid nitrogen in an automated physisorption instrument (Autosorb-iQ, Quantachrome Instruments). Prior to the analysis, the samples were outgassed under vacuum at 150 °C for 1.5 h.

2.2.3 Photocatalysis experiments

The photodegradation efficiency of all synthesized TiO_2 photocatalysts was tested towards decontamination of Rhodamine-B (RhB) and Methyl orange (MO) under solar light radiation. Initially stock solutions of 1 g/L were prepared by dissolving 1 g of RhB/MO in 1000 mL of double distilled water. In a typical experiment, 10 mg of catalyst was added to 100 mL of 20 mg L^{-1} RhB/MO solution in a 250 mL of beaker. Before irradiation, the suspension was magnetically stirred in dark for 1 h to ensure the establishment of the adsorption/desorption equilibrium of the dye onto the surface of photocatalysts. Afterwards the dye solution along with nanofiber was exposed to sunlight with continuous stirring. All the experiments were performed during the month of December and January (sunny days), from 11:00 AM to 12:30 PM, when the average solar intensity was 0.25 kW m^{-2} with minimum fluctuation. During photoreaction 5 mL of the suspension was collected at 15 min time intermission and centrifuged to eradicate the particles. After that the RhB/MO concentration in the solution was analyzed by UV–VIS spectrometer (Shimadzu spectrometer, model-2450) at its maximum adsorption wavelength (λ_{max}) of 554 nm for RhB and 463 nm for MO. This degradation method was continued till complete degradation of dye from the aqueous media.

3 Results and discussion

3.1 Characterization and properties of the prepared nanofibers

3.1.1 XRD analysis

The creation, crystalline phase, and purity of electrospun TiO_2 nanofibers were identified with XRD analysis. Figure 1 shows the XRD pattern of as-spun PVP/TIP nanofiber and calcined TiO_2 nanofiber. The as-spun PVP/TIP nanofiber (Fig. 2a) is amorphous, as characterized by the broad peak centered on 2θ = 25°. The XRD pattern of TiO_2 nanofibers obtained after calcination of PVP/TiO_2 nanofibers at 500 °C (Fig. 1b) exhibited characteristic reflections at 2θ values of 25.40°, 38.011°, 38.67°, 48.06°, 54.03°, 54.93°, 62.70°, 69.07°, 70.53 and 75.12° corresponding to (101), (004), (112), (200), (105), (211), (204), (116), (220) and (215) planes of the anatase phase, correspondingly according to JCPDS number 73–1764 and peaks at 27.6 and 41.3 corresponding

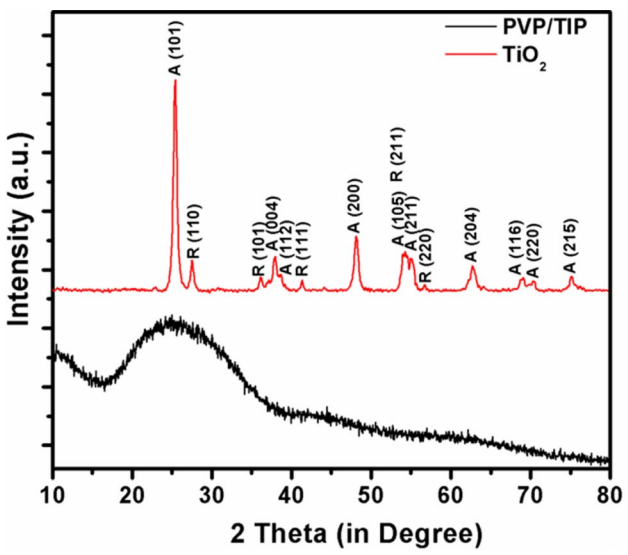

Fig. 1 XRD patterns of **a** PVP/TIP as-spun nanofiber and **b** TiO_2 nanofiber obtained after calcination at 500 °C

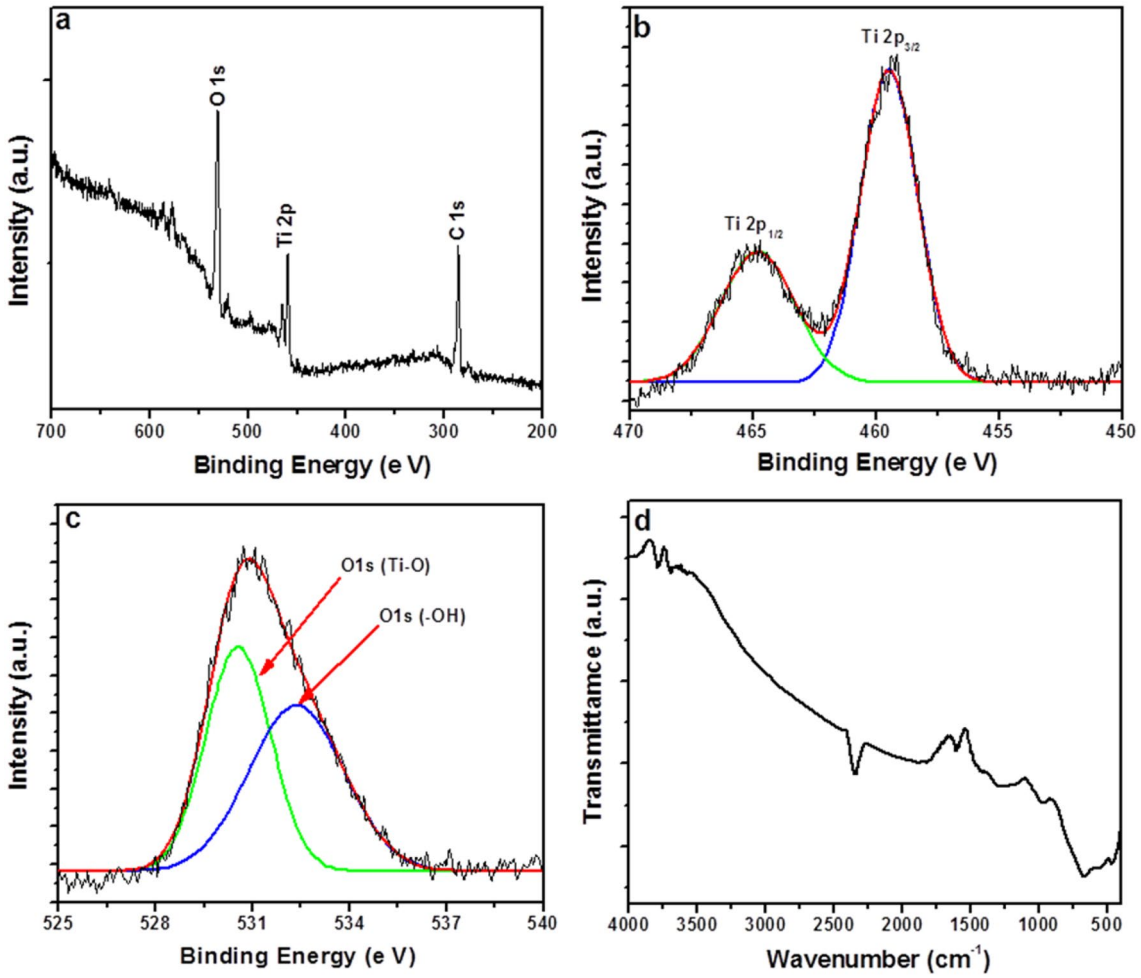

Fig. 2 XPS spectra of TiO_2 nanofiber: **a** survey; **b** Ti 2*p*; **c** O 1*s* and FTIR spectra of TiO_2 nanofiber

to rutile phase according to JCPDS number 78.1510. The XRD patterns confirmed the major presence of the anatase phase accompanied by a rather significant fraction of the rutile phase. No other significant peaks except the anatase and rutile phase of TiO_2 were identified; suggesting the formation of pure TiO_2.

3.1.2 XPS and FTIR analysis

More information on the elemental composition and chemical state of the calcined TiO_2 nanofibers is provided by XPS. The fully scanned spectra (Fig. 2a) show that the TiO_2 nanofibers contain Ti, O and C elements. The C element may be ascribed to an adventitious carbon-based contaminant. The high resolution XPS spectra of Ti 2*p* and O 1*s* are displayed in Fig. 2b, c. The Ti 2*p* spectrum of the TiO_2 nanofibers in Fig. 2b contains peaks at 459.4 and 464.9 eV, which correspond to Ti $2p_{3/2}$ and Ti $2p_{1/2}$, respectively. The peak separation between Ti $2p_{3/2}$ and Ti $2p_{1/2}$ peaks is 5.5 eV, suggesting the existence of the Ti^{4+} oxidation state [42]. In the O 1*s* region (Fig. 2c), binding energy values at 530.5 and 531.3 eV are observed. The binding energy value at 530.5 eV is corresponding to the characteristic peak of Ti–O–Ti. The other peak located at 531.6 is assigned to Ti–OH, which is due to surface adsorbed hydroxyl groups. The FTIR spectra of the TiO_2 nanofiber in the frequency range of 400–4000 cm^{-1} is shown in Fig. 2d. The existence of a peak corresponding to the stretching vibration of O–H and bending vibrations of adsorbed water molecules around 3200–3800 cm^{-1}, 2350 cm^{-1} and 1600 cm^{-1}, respectively. The broad intense band in the range of 450–700 cm^{-1} is due to the bending vibration of Ti–O bonds [43].

3.1.3 FESEM and EDS analysis

The surface morphology and elemental analysis of prepared electrospun PVP/TIP nanofibers and calcined TiO_2 nanofibers were investigated by FESEM and EDS and are presented in Fig. 3. The FESEM micrographs indicate that

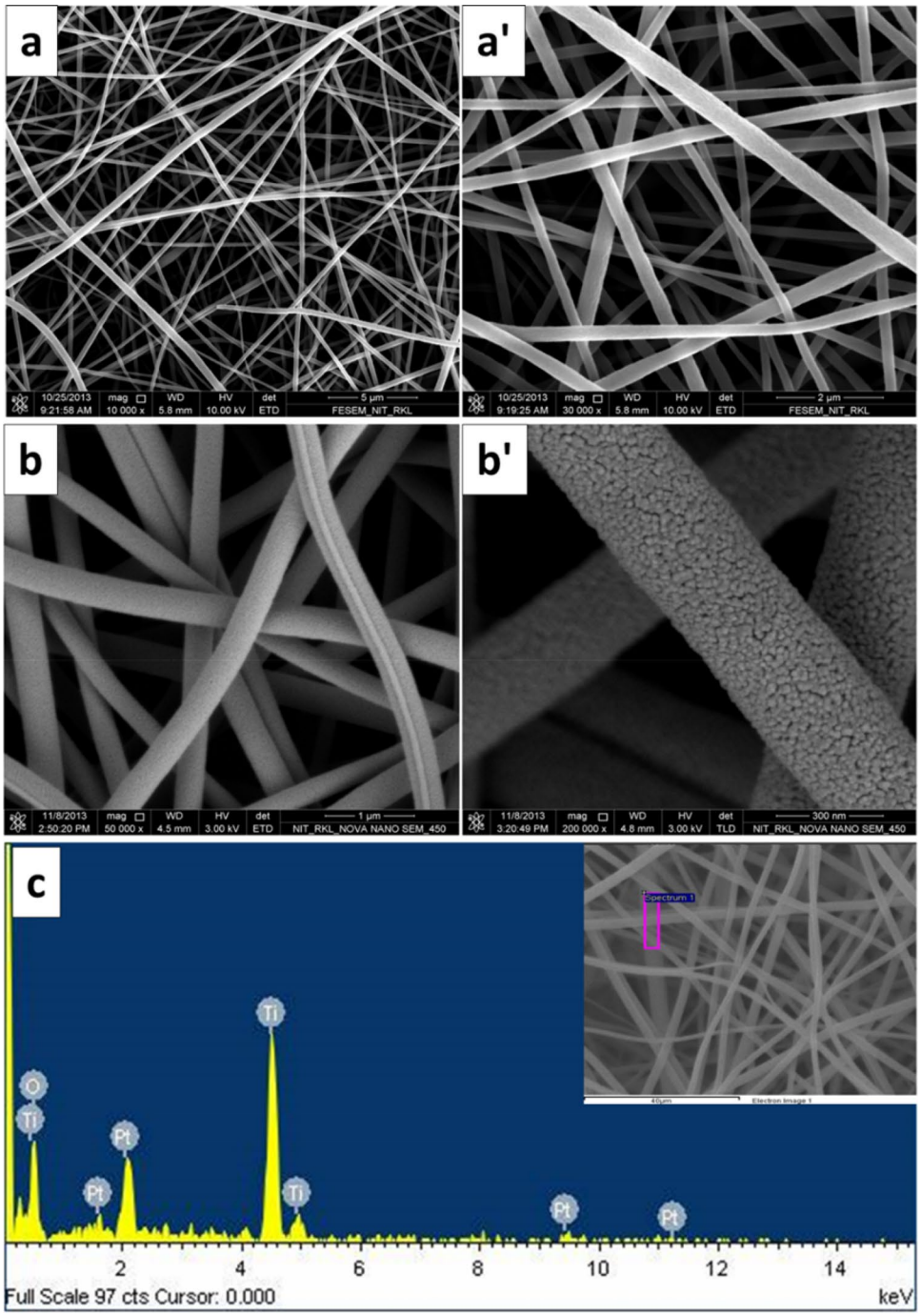

Fig. 3 FESEM images of **a**, **a**′ PVP/TIP as-spun nanofiber and **b**, **b**′ calcined TiO_2 nanofiber and **c** EDS of calcined TiO_2 nanofiber

all of the nanofibers contain continuous 1D structure. As can be seen from Fig. 3a, the PVP/TIP nanofibers are smooth and cylindrical in shape, the diameters were quite uniform (200–400 nm), and the surfaces of the fibers, shown in the magnified image of Fig. 3a′, were smoothly formed by the closely packed nanoparticles. Compared to the image of PVP/TIP, the images of TiO_2 (Fig. 3b, b′) show that subsequently calcination at 500 °C the fiber diameter and roughness of the fiber surface increased. The diameters of the calcined TiO_2 nanofiber are found to be in the range of 250–300 nm. From high magnified image it is observed that very fine tiny nanoparticles with diameter in the range of 10–20 nm are oriented along one dimensional direction to form the fibrous structure. The EDS analysis in Fig. 3c reveals the presence of oxygen and titanium elements in the calcined nanofibers.

3.1.4 TEM analysis

In order to obtain more information about the morphology, formation, and dimensions of individual TiO_2 ultrafine fibers, we have carried out TEM analysis. Figure 4a–c show TEM micrographs of TiO_2 ultrafine fibers. It was observed from TEM images that the particle diameters of the nanofibers were not uniform; instead, a range of fibers were formed (300–400 nm), which is also consistent with the fiber diameters as observed by the magnified FESEM micrographs. Figure 4d shows the selected-area electron diffraction pattern of titania nanofibers. The corresponding diffraction rings and bright spot on the electron diffraction pattern indicate the formation of highly crystalline TiO_2 fibers, which is also consistent with XRD results.

3.1.5 Surface area and porosity measurement

As observed from the high magnification (200,000×) FESEM images, the framework of a porous nanofiber is built up by loosely connected nanoparticles with average size around 10 nm. Figure 5a shows the N_2 adsorption–desorption isotherms of TiO_2 nanofiber. The fibers exhibit pronounced steep condensation step for relative pressures 0.2 to 0.4 arising from condensation of nitrogen inside the primary mesopores which is a characteristic of typical type IV adsorption/desorption isotherm. It clearly indicates that TiO_2 possesses a mesoporous structure. The surface area was found to be 161 m^2/g. Figure 5b shows the pore-size distribution plots calculated by the BJH equation from the desorption branch of the isotherm. Average pore diameter was found to be 12 nm; which further confirmed the mesoporous structure of the TiO_2 nanofibers.

3.2 Photocatalytic degradation of RhB and MO dye solutions under solar light irradiation

The photocatalytic activity of the prepared TiO_2 nanofiber was evaluated using the degradation of RhB and MO under solar light radiation by monitoring the intensity of the characteristic absorption peak at 554 nm of RhB and 463 of MO. The degradation percentage of the dyes was calculated by the equation:

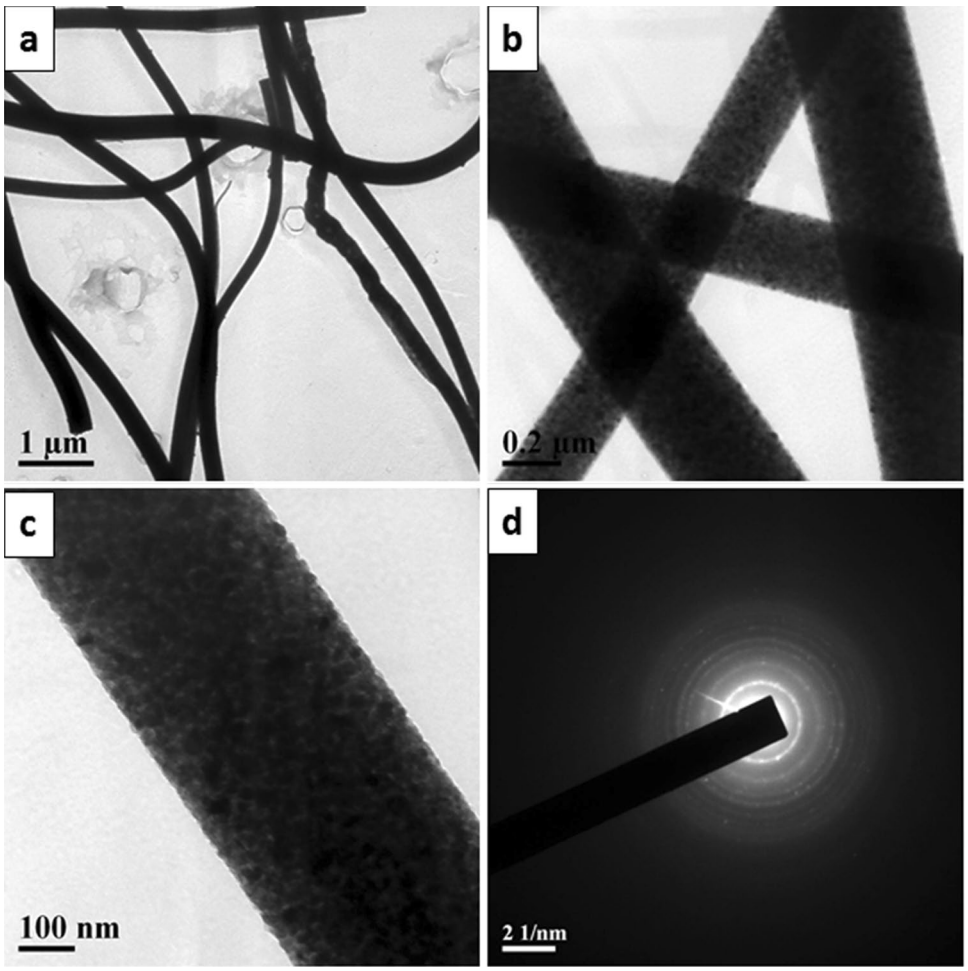

Fig. 4 **a**–**c** TEM images and **d** SAED pattern of calcined TiO_2 nanofiber

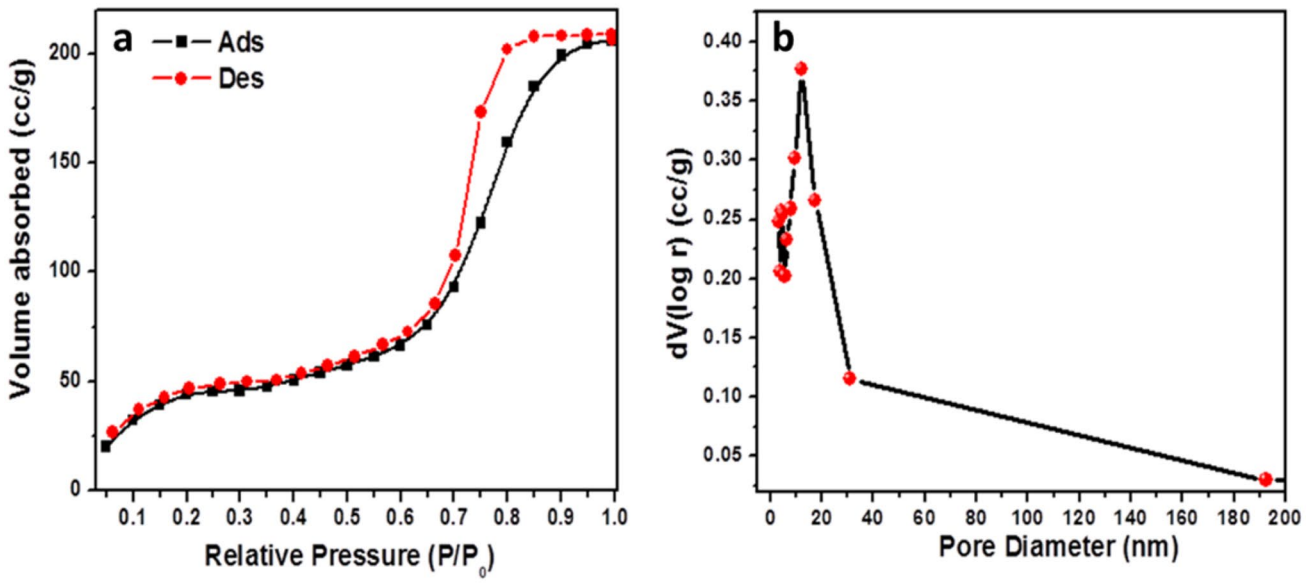

Fig. 5 Nitrogen adsorption desorption isotherm (**a**) and pore size distribution of TiO_2 Nanofibers

$$\text{Degradation percentage} = 100 \times \left(\frac{C_0 - C_t}{C_0}\right)\% = 100 \times \left(\frac{A_0 - A_t}{A_t}\right)\% \quad (1)$$

where C_0 and C_t were the concentration of the dye solution when the irradiation time was 0 and t and A_0 and at were the absorbance of the dye solution when the irradiation time was 0 and t, respectively. The UV–Vis spectral changes of RhB and MO aqueous solution in the process of photo degradation by TiO_2 nanofiber are displayed Fig. 6a, c, respectively. From the figure it is observed that, the absorbance of the dyes diminishes gradually with time elapsed and completely disappeared in 90 min. The photograph of the dye solutions before and after solar light radiation are given in Fig. 6b, d for RhB and MO, respectively; which also confirms the complete degradation of the dyes in 90 min.

Figure 7 shows the percentage of degradation of RhB and MO with time. For the photocatalytic experiments, the adsorption properties of the photocatalyst were initially studied. Prior to solar light irradiation, the reaction mixture was magnetically stirred for 60 min in dark in order to obtain percentage of adsorption, if any. The decrease in dye concentration due to adsorption was found to be around 4% for RhB and 1% for MO; this might be due to adsorption rather than photodecomposition. Conversely, through the exposure of solar light, the performances of the photoreaction were tremendously enhanced. After 90 min of solar light radiation the percentages of degradation of RhB and MO were found to be only 99.6 and 99.8%, respectively. We have also carried out the solar light irradiation experiment without photocatalyst. From the observation, it was confirmed that the degradation of the dyes was taken place due to the presence of TiO_2 nanofiber photocatalyst.

Using the Langmuir–Hinshelwood model, kinetics of the photo-degradation profile of RhB and MO dyes by electrospun TiO_2 nanofibers was determined. The equation is:

$$\ln\left(C_0/C_t\right) = K_1 t \quad (2)$$

where K_1 is pseudo first order rate constant (min^{-1}) and C_t is the concentration at time t. A plot of $\ln(C_0/C_t)$ versus t gives the value of K_1. The reaction rate constants (K_1) for all the three photocatalysts were determined from the slope of the fitted curves (Fig. 8) by means of linear regression and the values are given in Table 1. Good linear relationship between $\ln(C_0/C_t)$ and the radiation time is observed for both the dye solutions. The rate constant for RhB and MO were found to be 0.916 and 1.108 with good regression coefficients ($R^2 > 0.94$).

Catalyst lifetime is an important parameter of the photocatalytic process because its use for a longer period of time leads to a significant cost reduction of the treatment. The reusability of the 1D electrospun TiO_2 nanofiber as photocatalysts is also investigated by collecting and reusing the same photocatalyst for 4 multiple cycles for both the dyes and the result is shown in Fig. 9. As can be seen, the repeatability of the entire process and the final result of degradation of RhB and MO are very good, which further demonstrate the excellent efficiency of the photocatalyst. We have also repeated the photocatalytic

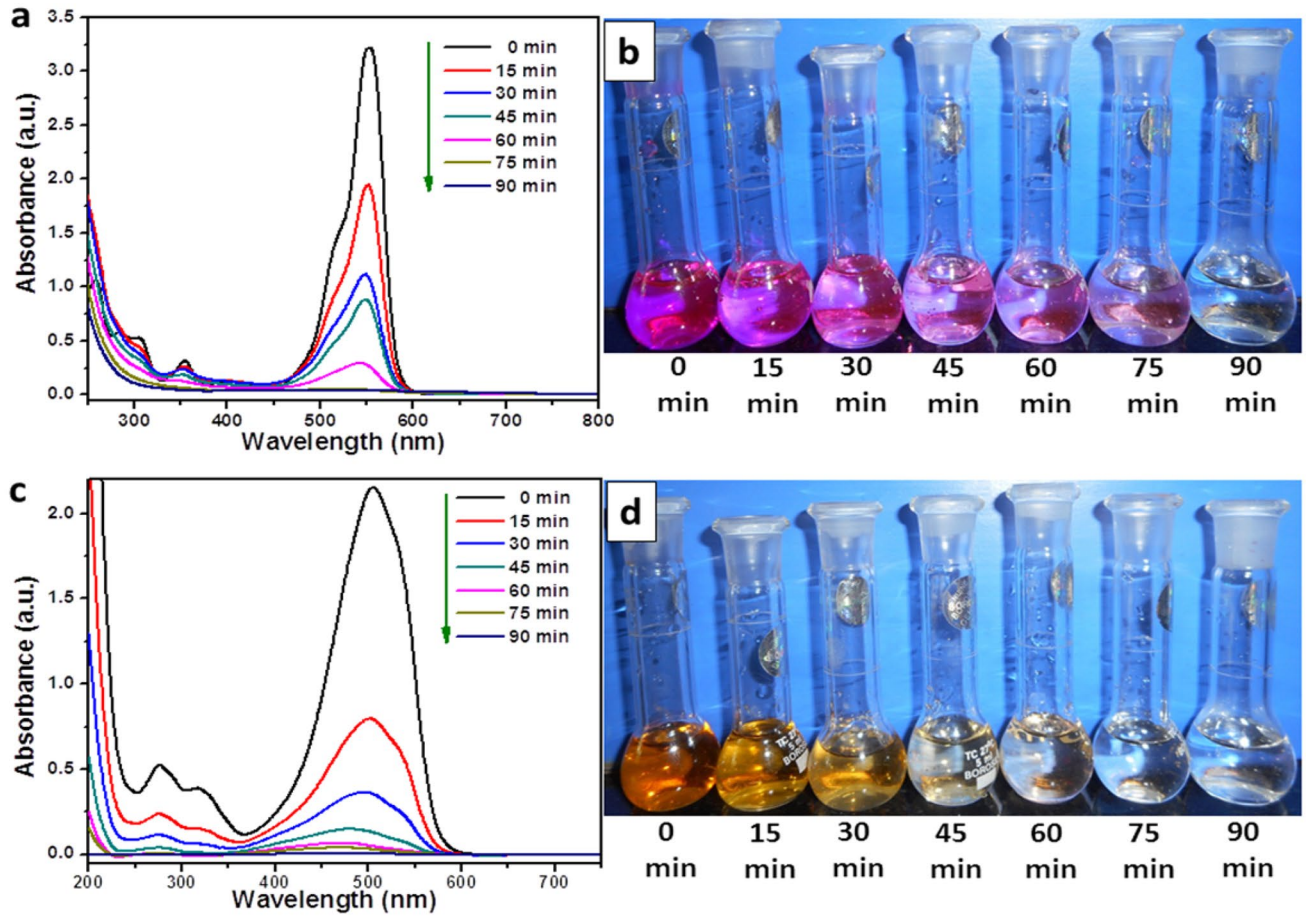

Fig. 6 UV–Vis spectral changes and optical images, **a**, **b** Rhodamine B and **c**, **d** methyl orange during degradation process as a function of reaction time using TiO_2 nanofibers (100 mL of 20 mg L^{-1} dye solution using 0.1 g catalyst each)

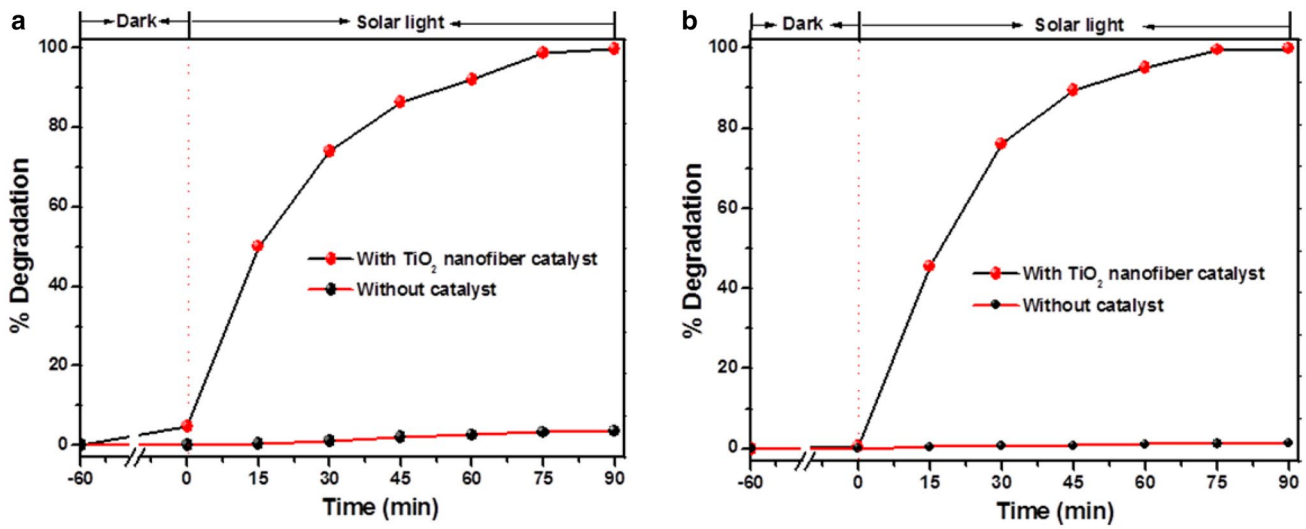

Fig. 7 Percentage of photodegradation, **a** Rhodamine B and **b** methyl orange dye solutions under solar light irradiation using 0.01 g TiO_2 nanofiber catalyst and without catalyst

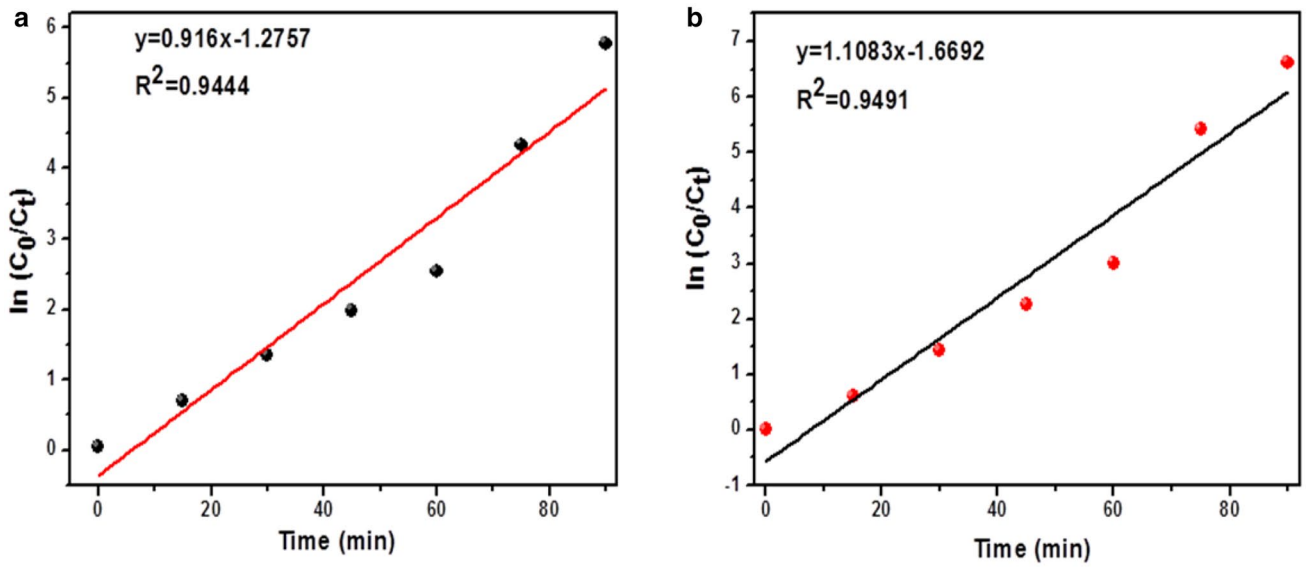

Fig. 8 Pseudo-first-order reaction kinetic linear relationship curves for degradation of **a** RhB and **b** MO by TiO_2 nanofibers under solar light irradiation

Table 1 Percentage of degradation and pseudo-first-order kinetic parameters

Dye	Degradation (%)	K_1 (min^{-1})	R^2
RhB	99.6	0.916	0.9444
MO	99.8	1.108	0.9491

experiments using real visible light source (quartz photochemical reactor fitted with 250 W high pressure mercury vapor lamp, equipped with cooling water circulation system). The result obtained is presented in the supporting information (Fig. S1). The prepared TiO_2 nanofibers photocatalyst is found to degrade 99.8% of MO dye under real visible light within 75 min of contact time.

Furthermore, we have carried out the visible light photocatalytic degradation of non-colored tetracycline hydrochloride (20 mg/L) compound. It is observed that the TiO_2 photocatalyst is efficiently degrading (98%) the tetracycline hydrochloride solution within 70 min of contact time (supporting information, Fig. S2). The obtained result suggests that the prepared TiO_2 nanofibers are efficient visible

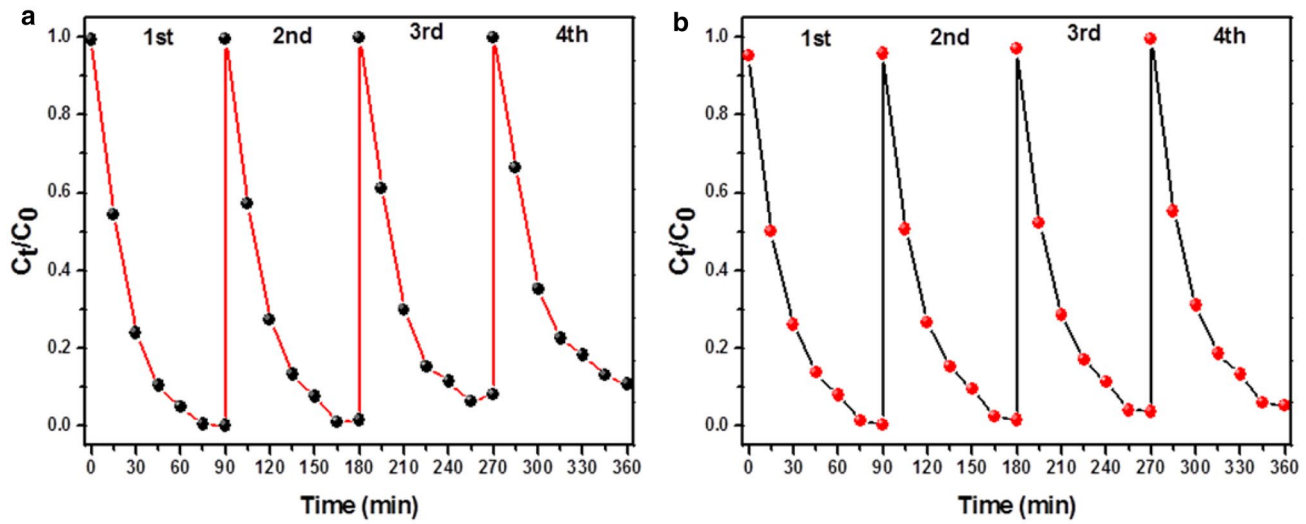

Fig. 9 Repeating experiments for the photocatalytic degradation of **a** RhB and **b** MO using TiO_2 nanofiber under solar light irradiation

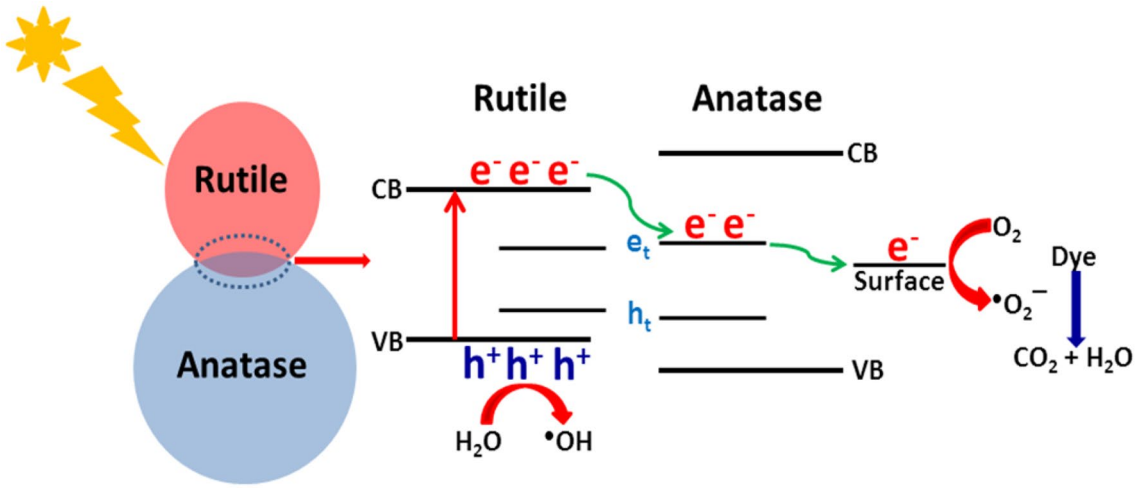

Fig. 10 Proposed schematic illustrations showing the reaction mechanism for photocatalytic degradation of organic pollutants under visible light irradiation

light active photocatalyst and can be used for photocatalytic degradation of toxic organic compounds.

3.3 Photocatalytic mechanism

Three major factors depend upon the efficiency of a metal oxide photocatalyst are charge separation, charge recombination and charge transport to the surface. For higher photocatalytic activity, one should facilitate charge separation and transfer while inhibiting charge recombination [44]. Here, the synthesized TiO_2 nanofibers exhibit dual phase i.e. major anatase and minor rutile phase. Generally, the rutile phase possesses high rates of recombination and lesser photocatalytic active compared to the anatase. But in our case due to interwoven of small rutile crystallites with anatase crystallites, efficient electron transfer occurs at the anatase–rutile interface (described in Fig. 10). The rutile phase spreads the photoactive range into the visible, gathering more light, and electron transfer from rutile to anatase trapping sites hinders charge recombination [45]. The schematic illustration of proposed mechanism is shown in Fig. 10. The presence of small amount of rutile crystallites would create a structure where rapid electron transfers from rutile to lower energy anatase lattice trapping sites under solar light irradiation, which leads to a more stable charge separation. The photo generated electrons transform from rutile to lattice trapping sites of anatase and hence the holes without recombination reach the surface. Again, the electrons from the anatase trapping sites move to surface trapping sites, further separating the electron/hole pair [45, 46]. The well-ordered and aligned TiO_2 particle assembly is an ideal structure to enhance the separation of electron–hole charge pairs and facilitate inter particle charge transfer. In addition, the mesoporous structure created via the TiO_2 particle–particle interconnection is very advantageous in enhancing the adsorption of reactants and desorption of products [44]. From FESEM image (Fig. 3b′), it is observed that a single TiO_2 nanofiber consists of compactly packed spherical particles of around 10–20 nm in diameter that form a cylinder-type fiber of around 300–500 nm in diameter and a few micrometers in length. Hence, a very rapid interparticle, vectorial transport of photogenerated charge carriers (electrons–holes) is likely to occur through the grain boundaries [44].

In order to inspect photogenerated electron transfer pathways, we have carried out the photoluminescence (PL) emission spectra of the prepared TiO_2 nanofibers by exciting at wavelengths of 350 nm. The PL spectrum is associated to the transfer behavior of the photoinduced electrons and holes so that it can reflect the separation and recombination rate of photoinduced charge carriers. The result obtained from photo luminesce (PL) experiments is presented in the supporting information (Fig. S2). Very low PL intensity in case of mixed TiO_2 nanofibers is due to the efficient separation of photo induced electron–holes charge carriers.

4 Conclusion

PVP/TIP composite nanofibers were fabricated via electrospinning technology using a solution of Titanum-isopropoxide (TIP) and Polyvinylpyrrolidone (PVP) precursors in ethanol. Then the PVP/TIP composite nanofibers were calcined at 500 °C to form mixed phase mesoporous TiO_2 nanofibers. XRD analysis confirmed the major presence of the anatase phase accompanied by a rather significant fraction of the rutile phase. From FESEM and TEM

analysis, it is observed that very fine tiny nanoparticles with diameter in the range of 10–20 nm are oriented along one dimensional direction to form the fibrous structure with diameter in the range of 300–500 nm. The prepared dual phase TiO_2 nanofibers exhibit superb photocatalytic activity for the degradation of toxic dyes Rhodamine B and methyl orange under solar light irradiation. The excellent visible light photocatalytic activity may be attributed to the combine factors of heteroconjuction at anatase–rutile interface and immediate charge transfer due to 1D structure, which inhibit the electron–hole recombination.

Acknowledgements Dr. Dhal is thankful to NIT Rourkela, and MHRD, Govt. of India for providing research facility and infrastructure to carry out this works in the form of an Institute fellowship (SRF).

Compliance with ethical standards

Conflict of interest The authors declare that they have no conflict of interest.

References

1. Jiang DB, Yuan Y, Zhao D, Tao K, Xu X, Zhang YX (2018) Facile synthesis of three-dimensional diatomite/manganese silicate nanosheet composites for enhanced Fenton-like catalytic degradation of malachite green dye. J Nanopart Res 20:123. https://doi.org/10.1007/s11051-018-4226-2
2. Li Y, Dong S, Zhu L (2018) Preparation of novel poly(vinylidene fluoride)/TiO_2 photocatalysis membranes for use in direct contact membrane distillation. J Nanopart Res 20:63. https://doi.org/10.1007/s11051-018-4167-9
3. Subramaniam MN, Goh PS, Abdullah N, Lau WJ, Ng BC, Ismail AF (2017) Adsorption and photocatalytic degradation of methylene blue using high surface area titanate nanotubes (TNT) synthesized via hydrothermal method. J Nanopart Res 19:220. https://doi.org/10.1007/s11051-017-3920-9
4. Wang S, Li D, Sun C, Yang C, Guan Y, He H (2014) Synthesis and characterization of g-C_3N_4/Ag_3VO_4 composites with significantly enhanced visible-light photocatalytic activity for triphenylmethane dye degradation. Appl Catal B Environ 144:885–892
5. Wang X, Xiong W, Li X, Zhao Q, Fan S, Zhang M, Mu J, Chen A (2018) Fabrication of MoS_2@g-C_3N_4 core–shell nanospheres for visible light photocatalytic degradation of toluene. J Nanopart Res 20:243
6. Doh SK, Kim C, Lee SG, Lee SJ, Kim H (2008) Development of photocatalytic TiO_2 nanofibers by electrospinning and its application to degradation of dye pollutants. J Hazard Mater 154:118–127
7. Long B, Chen S, Wang B, Tang J, Yang J, Zhou X (2018) A facile synthesis of heteroatom-doped carbon framework anchored with TiO_2 nanoparticles for high performance lithium ion battery anodes. J Nanopart Res 20:164. https://doi.org/10.1007/s11051-018-4263-x
8. Wang Q, Zhu S, Liang L, Cui Z, Yang X, Liang C, Inoue A (2017) Synthesis of Br-doped TiO_2 hollow spheres with enhanced photocatalytic activity. J Nanopart Res 19:72. https://doi.org/10.1007/s11051-017-3765-2
9. Saif M, Aboul-Fotouh SMK, El-Molla SA, Ibrahim MM, Ismail LFM (2012) Improvement of the structural, morphology, and optical properties of TiO_2 for solar treatment of industrial wastewater. J Nanopart Res 14:1227
10. Dai K, Peng T, Chen H, Liu J, Zan L (2009) photocatalytic degradation of commercial phoxim over La-doped TiO_2 nanoparticles in aqueous suspension. Environ Sci Technol 43:1540–1545
11. Devi LG, Murthy MN (2008) Characterization of Mo doped TiO_2 and its enhanced photo catalytic activity under visible light. Catal Lett 125(3–4):320–330
12. Goswami P, Ganguli JN (2013) Tuning the band gap of mesoporous Zr-doped TiO_2 for effective degradation of pesticide quinalphos. Dalton Trans 42:14480–14490. https://doi.org/10.1039/C3DT51891D
13. Singla P, Pandey OP, Singh K (2016) Study of photocatalytic degradation of environmentally harmful phthalate esters using Ni-doped TiO_2 nanoparticles. Int J Environ Sci Technol 13:849–856
14. Tabasideh S, Maleki A, Shahmoradi B, Ghahremani E, McKay G (2017) Sonophotocatalytic degradation of diazinon in aqueous solution using iron-doped TiO_2 nanoparticles. Sep Purif Technol 189:186–196
15. An Y, Ridder DD, Zhao C, Schoutteten K, Bussche JV, Zheng H, Chen G, Vanhaecke L (2016) Adsorption and photocatalytic degradation of pharmaceuticals and pesticides by carbon doped-TiO_2 coated on zeolites under solar light irradiation. Water Sci Technol 73:2868–2881
16. Barkul RP, Patil MK, Patil SM, Shevale VB, Delekar SD (2017) Sunlight-assisted photocatalytic degradation of textile effluent and Rhodamine B by using iodine doped TiO_2 nanoparticles. J Photochem Photobiol A Chem 349:138–147. https://doi.org/10.1016/j.jphotochem.2017.09.011
17. Cordero-García A, Palomino GT, Hinojosa-Reyes L, Guzmán-Mar JL, Maya-Teviño L, Hernández-Ramírez A (2017) Photocatalytic behaviour of WO_3/TiO_2-N for diclofenac degradation using simulated solar radiation as an activation source. Environ Sci Pollut Res 24:4613–4624. https://doi.org/10.1007/s11356-016-8157-0
18. Quinones DH, Rey A, Alvarez PM, Beltran FJ, Puma GL (2015) Boron doped TiO_2 catalysts for photocatalytic ozonation of aqueous mixtures of common pesticides: diuron, o-phenylphenol, MCPA and terbuthylazine. Appl Catal B Environ 178:74–81. https://doi.org/10.1016/j.apcatb.2014.10.036
19. Chaker H, Chérif-Aouali L, Khaoulani S, Bengueddach A, Fourmentin S (2016) Photocatalytic degradation of methyl orange and real wastewater by silver doped mesoporous TiO_2 catalysts. J Photochem Photobiol A Chem 318:142–149. https://doi.org/10.1016/j.jphotochem.2015.11.025
20. Lannoy A, Bleta R, Machut-Binkowski C, Addad A, Monflier E, Ponchel A (2017) Cyclodextrin-directed synthesis of gold-modified TiO_2 materials and evaluation of their photocatalytic activity in the removal of a pesticide from water: effect of porosity and particle size. ACS Sustain Chem Eng 5:3623–3630
21. Yu J, Qi L, Jaroniec M (2010) Hydrogen production by photocatalytic water splitting over Pt/TiO_2 nanosheets with exposed (001) facets. J Phys Chem C 114:13118–13125
22. He Z, Cai Q, Wu M, Shi Y, Fang H, Li L, Chen J, Chen J, Song S (2013) Photocatalytic reduction of Cr(VI) in an aqueous suspension of surface-fluorinated anatase TiO_2 nanosheets with exposed 001 facets. Ind Eng Chem Res 52:9556–9565
23. Yu J, Low J, Xiao W, Zhou P, Jaroniec M (2014) Enhanced photocatalytic CO_2-reduction activity of anatase TiO_2 by coexposed 001 and 101 facets. J Am Chem Soc 136:8839–8842
24. Cheng WY, Yu TH, Chao KJ, Lu SY (2014) Cu_2O-decorated mesoporous TiO_2 beads as a highly efficient photocatalyst for hydrogen production. Chem Cat Chem 6:293. https://doi.org/10.1002/cctc.201300681

25. Hernández S, Cauda V, Chiodoni A, Dallorto S, Sacco A, Hidalgo D, Celasco E, Pirri CF (2014) Optimization of 1D ZnO@TiO_2 core–shell nanostructures for enhanced photoelectrochemical water splitting under solar light illumination. ACS Appl Mater Interfaces 6:12153–12167
26. Hung W-H, Chien T-M, Tseng C-M (2014) Enhanced photocatalytic water splitting by plasmonic TiO_2–Fe_2O_3 cocatalyst under visible light irradiation. J Phys Chem C 118:12676–12681
27. Kim J, Kang M (2012) High photocatalytic hydrogen production over the band gap-tuned urchin-like Bi_2S_3-loaded TiO_2 composites system. Int J Hydrog Energy 37:8249–8256
28. Sharma M, Vaidya S, Ganguli AK (2017) Enhanced photocatalytic activity of g-C_3N_4–TiO_2 nanocomposites for degradation of Rhodamine B dye. J Photochem Photobiol A Chem 335:287–293
29. Zhou W, Liu X, Cui J, Liu D, Li J, Jiang H, Wang J, Liu H (2011) Control synthesis of rutile TiO_2 microspheres, nanoflowers, nanotrees and nanobelts via acid-hydrothermal method and their optical properties. Cryst Eng Commun 13:4557–4563
30. Zhang X, Xu S, Han G (2009) Fabrication and photocatalytic activity of TiO_2 nanofiber membrane. Mater Lett 63:1761–1763
31. Lee E, Hong JY, Kang H, Jang J (2012) Synthesis of TiO_2 nanorod-decorated graphene sheets and their highly efficient photocatalytic activities under visible-light irradiation. J Hazard Mater 219–220:13–18
32. Zhang Z, Shao C, Li X, Zhang L, Xue H, Wang C, Liu Y (2010) Electrospun nanofibers of ZnO–SnO_2 heterojunction with high photocatalytic activity. J Phys Chem C 114:7920–7925
33. Hu G, Meng X, Feng X, Ding Y, Zhang S, Yang M (2007) Anatase TiO_2 nanoparticles/carbon nanotubes nanofibers: preparation, characterization and photocatalytic properties. J Mater Sci 42:7162–7170
34. Chen YL, Chang YH, Huang JL, Chen I, Kuo C (2012) Light scattering and enhanced photoactivities of electrospun titania nanofibers. J Phys Chem C 116:3857–3865
35. Kumar A, Jose R, Fujihara K, Wang J, Ramakrishna S (2007) Structural and optical properties of electrospun TiO_2 nanofibers. Chem Mater 19:6536–6542
36. Zhang X, Thavasi V, Mhaisalkar SG, Ramakrishna S (2012) Novel hollow mesoporous 1D TiO_2 nanofibers as photovoltaic and photocatalytic materials. Nanoscale 4:1707–1716
37. Xu F, Xiao W, Cheng B, Yu J (2014) Direct Z-scheme anatase/rutile bi-phase nanocomposite TiO_2 nanofiber photocatalyst with enhanced photocatalytic H_2-production activity. Int J Hydrog Energy 39:15394–15402
38. Wang C, Zhang X, Shao C, Zhang Y, Yang J, Sun P, Liu X, Liu H, Liu Y, Xie T, Wang D (2011) Rutile TiO_2 nanowires on anatase TiO_2 nanofibers: a branched heterostructured photocatalysts via interface-assisted fabrication approach. J Colloid Interface Sci 363:157–167
39. Zhang X-Y, Li H-P, Cui X-L, Lin Y (2010) Graphene/TiO_2 nanocomposites: synthesis, characterization and application in hydrogen evolution from water photocatalytic splitting. J Mater Chem 20:2801–2806
40. Zhang Z, Shao C, Li X, Wang C, Zhang M, Liu Y (2010) Electrospun nanofibers of p-type NiO/n-Type ZnO heterojunctions with enhanced photocatalytic activity. ACS Appl Mater Interfaces 2:2915–2923
41. Liu H, Yang J, Liang J, Huang Y, Tang C (2008) ZnO nanofiber and nanoparticle synthesized through electrospinning and their photocatalytic activity under visible light. J Am Ceram Soc 91:1287–1291
42. Su C, Liu L, Zhang M, Zhang Y, Shao C (2012) Fabrication of Ag/TiO_2 nanoheterostructures with visible light photocatalytic function via a solvothermal approach. Cryst Eng Commun 14:3989–3999
43. Bineesh VK, Kim D-K, Park D-W (2010) Doped nanostructures. Nanoscale 2:1057
44. Choi SK, Kim S, Lim SK, Park H (2010) Photocatalytic comparison of TiO_2 nanoparticles and electrospun TiO_2 nanofibers: effects of mesoporosity and interparticle charge transfer. J Phys Chem C 114:16475–16480
45. Hurum DC, Agrios AG, Gray KA, Rajh T, Thurnauer MC (2003) Explaining the enhanced photocatalytic activity of Degussa P25 mixed-phase TiO_2 using EPR. J Phys Chem B 107:4545–4549
46. Liu B, Peng L (2013) Facile formation of mixed phase porous TiO_2 nanotubes and enhanced visible-light photocatalytic activity. J Alloys Compd 571:145–152

Publisher's Note Springer Nature remains neutral with regard to jurisdictional claims in published maps and institutional affiliations.